



ORIGINAL ARTICLE

Artemisinin-loaded silk fibroin/gelatin composite hydrogel for wound healing and tumor therapy



Yu Bao, Hai-qiang Zhang, Li Chen, Hai-Hua Cai, Zu-Lan Liu, Yan Peng, Zhi Li^{*}, Fang-Yin Dai^{*}

^a State Key Laboratory of Silkworm Genome Biology, Southwest University, Chongqing 400715, China

^b College of Sericulture, Textile and Biomass Sciences, Southwest University, Chongqing 400715, China

Received 19 January 2023; accepted 1 March 2023

Available online 8 March 2023

KEYWORDS

Artemisinin;
Silk fibroin;
Gelatin;
Wound healing;
Antitumor

Abstract As a natural extract with multiple pharmacological activities, the application of artemisinin (ART) is limited by poor solubility, short half-life and first-pass effect. In this study, ART was loaded into a drug delivery system based on silk fibroin and gelatin to develop a composite hydrogel for wound healing and cancer therapy. With crosslinked by genipin, the fabricated SF-G-ART hydrogel had good flexibility and ductility, its tensile strength was 1.42 MPa and the maximum elongation could reach 124.99%. Within 120 h, SF-G-ART hydrogel cumulatively released 81.74% of ART. The release effect of this hydrogel could be controlled by pH. The fabricated SF-G-ART hydrogel exhibited anti-inflammatory effect and anti-cancer cell property. The further animal experiment showed that it could shorten the inflammatory process and accelerated the repair of wound tissue. Moreover, with the release of ART, SF-G-ART hydrogel could significantly inhibit the tumor growth *in vivo*. These findings demonstrate that the fabricated SF-G-ART hydrogel in this study has a good potential for application in wound healing and cancer therapy.

© 2023 The Authors. Published by Elsevier B.V. on behalf of King Saud University. This is an open access article under the CC BY-NC-ND license (<http://creativecommons.org/licenses/by-nc-nd/4.0/>).

1. Introduction

Biomaterials play an important role in the field of biomedicine (Kumar et al., 2020a), and hydrogels are one of the main manifestations. Hydrogels constructed by three-dimensional network polymers exhibit excellent physical, chemical, biological properties, and they are widely used in the fields of tissue engineering, drug sustained-release systems, wastewater treatment, actuators, sensors, and electronics (Kumar and Jaiswal, 2016; Capanema et al., 2018). Wound dressings is a main application for hydrogels in the biomedical field. Hydrogels can provide a hypoxic environment for wounds, which is beneficial for capil-

lary formation. Their good swelling performance allows them to absorb exudates and remove necrotic tissue and toxins from wound, accelerating the wound healing (Zhang, 2020; Huang et al., 2021).

Hydrogels, made from macromolecule polymers especially natural polymers, generally have excellent biological properties, and they can be safely used in the biomedical field (Ahmadian et al., 2019; Eftekhari et al., 2020). Silk fibroin (SF) and gelatin (G) have been widely used in the preparation of hydrogels as natural protein polymers (Kapoor and Kundu, 2016). SF, a natural polymer material extracted from silk, has unique mechanical properties and biological characteristics. SF-based biomaterials are highly biocompatible *in vitro* and *in vivo* (Dong et al., 2021). SF based hydrogels have been used as drug delivery systems to deliver the anticancer drug (doxorubicin) for the treatment of breast cancer (Florczak et al., 2021). G is a natural protein hydrolyzed from collagen, and it has good

^{*} Corresponding authors.

E-mail addresses: tlizhi@swu.edu.cn (Z. Li), fydai@swu.edu.cn (F.-Y. Dai).

biocompatibility and biodegradability. The arginine-glycine-aspartic acid sequence (RGD) contained in G hydrogel has an ability to regulate cell adhesion (Yoon et al., 2016). G-based hydrogel can promote wound collagen sedimentation as a wound dressing, and it can also deliver related drugs such as chemokines to the target site as a drug loading system (Broderick et al., 2005). However, hydrogel prepared by a single component, no matter G or SF, usually has shortcomings in property, such as poor stability at high temperature and weak mechanical performance, which limits its practical applications (Guo et al., 2021). These problems likely be solved by a composite hydrogel (Xie et al., 2018; Kumar et al., 2020b). Genipin is a natural crosslinking agent from the scorpion fruit of the *Rubiaceae* plant (Sung et al., 2001). It can combine with amino groups in polymer materials to form a covalent network, forming a three-dimensional network structure inside. Moreover, genipin has the property of anti-allergy and anti-inflammation, making it more suitable for hydrogel dressing (Koo et al., 2006). In this study, genipin was used as a crosslinking agent for strengthening the combination of these two natural protein polymers and improving mechanical properties.

For purpose of antimicrobial effect, antibacterial agents are loaded on hydrogel. Antibiotics and metal ions are widely used because of their good antibacterial activity. Neomycin and moxifloxacin were loaded on tragacanth gum based sterile hydrogel respectively to fabricate wound dressing, and both hydrogels exhibited good antimicrobial activity (Singh et al., 2016a). Ag together with graphene was loaded on polymer hydrogel, and the fabricated hydrogel could effectively kill bacteria and accelerate wound healing (Fan et al., 2014). Recently, antibacterial agents from natural extracts without induction of drug resistance attract increasingly attention in recent years. Artemisinin (ART), extracted from the stems and leaves of *Artemisia annua*, is a sesquiterpene lactone compound with peroxy groups (Barradell and Fitton, 1995). ART is well-known as its excellent antimalarial property. Moreover, ART also has reported inhibitive effect on some types of cancer cells and immune diseases, including breast cancer cell (Natesan et al., 2017), cervical cancer cell (Luo et al., 2014), systemic lupus erythematosus (Wu et al., 2016). Different from traditional medicines, the mechanism of ART is that peroxy groups are cleaved by intracellular substances to generate free radicals which then destroys biological macromolecules inside bacteria and cancer cells (Mocini et al., 2020; Sharma et al., 2021). The high content of the mediators (Fe^{2+}) in cancer cells makes ART selective (Li et al., 2018). However, ART has hardly been used for relative therapy so far due to the short half-life and poor water solubility. The combined use of ART and Polyethylene glycol (PEG) can improve the water solubility of ART (Dai et al., 2020). As a drug sustained-release system, hydrogel is a suitable choice for loading ART and releasing it after then.

In this work, to fabricate hydrogel with improved mechanical property for application in wound healing and cancer therapy, ART was dissolved in PEG4000 for improving solubility, and then it was used to fabricate composite SF-G-ART hydrogel together with SF and G (Fig. 1). The content ratio of hydrogel was optimized by taking the releasing effect of ART as a response value according to response surface analysis (RSM). The optimized hydrogel exhibited a porous structure with good mechanical properties, swelling properties and thermal stability. The loaded ART could be sustained release and this process was pH responsive. The sustained-released ART had significant anti-inflammatory and anti-tumor properties, and the composite hydrogel could be used for wound healing and cancer therapy *in vivo*.

2. Material and methods

2.1. Material

ART (purity > 98%), PEG4000, gelatin and genipin were purchased from Shanghai Aladdin Biochemical Technology Co.,

Ltd (Shanghai, China). Analytically pure Na_2CO_3 , CaCl_2 , $\text{C}_2\text{H}_5\text{OH}$, $\text{SnCl}_2 \cdot 2\text{H}_2\text{O}$, NaOH , $\text{Na}_3\text{C}_6\text{H}_5\text{O}_7$, 2,2-Dihydroxyindane-1,3-dione (IUPAC), *iso*-Propyl alcohol (IPA) were purchased from Chongqing Chuandong Chemical Co., Ltd (Chongqing, China). Dulbecco's modified Eagle's medium (DMEM), Trypsin-EDTA (0.25%) and PBS were acquired from Gibco BRL, Rockville, MD, United States. 3-[4,5-dimethylthiazol-2-yl]-5-[3-carboxymethoxyphenyl]-2-[4-sulfophenyl]-2H-tetrazolium, inner salt (MTS) was purchased from Promega, Beijing, China. LIVE/DEAD BacLight Bacterial Viability Kit was purchased from Molecular Probes Inc. Lipopolysaccharides (LPS, from *E. coli*) and Micro NO Content Assay Kit were acquired from Solarbio, Beijing, China.

2.2. Preparation of SF-G-ART

SF (2%, w/v) was extracted from quantitative silk by degumming-drying-dissolving in ternary solution-dialyzing. A higher concentration of SF was prepared by reverse osmosis in PEG20000 (20%, w/v) solution for 24 h. The SF solution was incubated at 60 °C for 24 h and then diluted with deionized water to a target concentration. Make an ART solution based on previous experiments: Quantitative ART was weighted and dissolved in ethanol solution to form 1 mg/mL ART ethanol solution. The ART ethanol solution and the 12% PEG4000 aqueous solution were mixed at 1:1 (v/v), and the mixture was stirred under a magnetic stirrer for 2 h at 37 °C. In the case, the alcohol in mixed solution was naturally volatilized and then the mixed solution was made up to a concentration of 1 mg/mL of ART in distilled water. The G powder was dissolved with stirring in ART solution at 40 °C for 1 h to become homogeneous G solution. Genipin was sonicated in 60% ethanol solution to obtain genipin solution (1%, w/v). The SF and G solution were equal volume mixed, and vortexed for 3 min. Genipin solution with different ratios was added into the SF/G blends and then mixed by vortexing for 5 min. The mixed solution placed in polyethylene Petri dishes was crosslinked at 37 °C for 24 h to finally obtain a composite hydrogel (SF-G-ART). SF-G hydrogel fabricated by the same method without loading ART is set as control.

2.3. Experimental design

To optimize the drug sustained-release ability of the hydrogel, we set different concentration of each component suitable for fabricating the hydrogel. And then, the response surface method (RSM) was used to optimize the hydrogel formulation. SF concentration (A), G concentration (B), and crosslinking ratio (C, ratio of total substance content and crosslinking agent) were taken as independent variables (factors) in RSM (Table 1). The variation levels were divided into low (−1), medium (0) and high (1). The drug release rate of the hydrogel in PBS (pH7.4) was taken as the dependent variable (response). Statistical analysis and protocol optimization were achieved through Design Expert Software to obtain the optimal hydrogel synthesis.

2.4. Morphology and composition analysis of hydrogels

The SF-G-ART and SF-G were frozen overnight and then lyophilized for 24 h (LyoQuest, Telstar, Spain). The dried samples

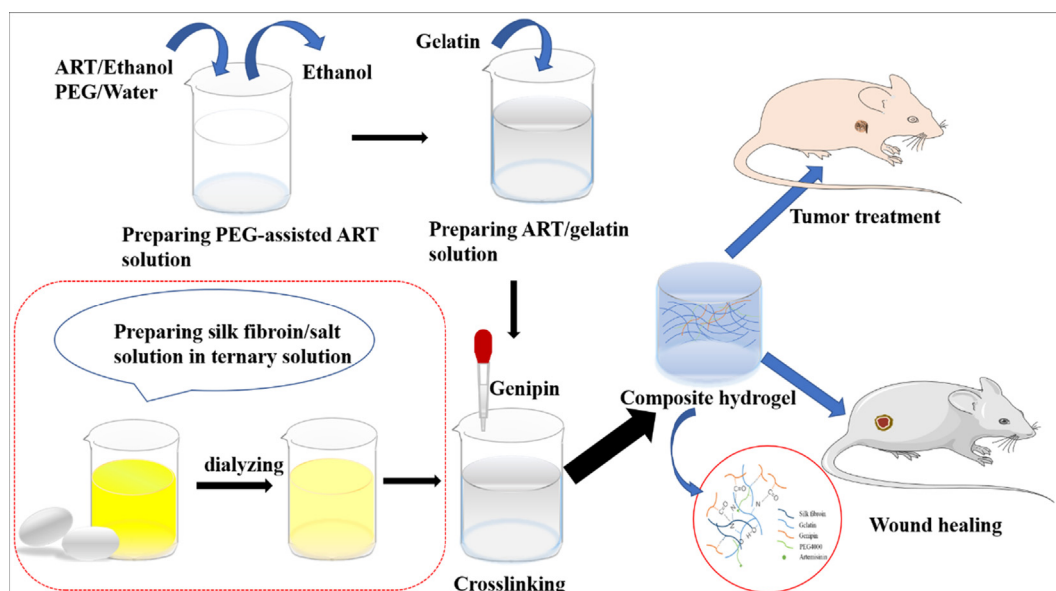


Fig. 1 Schematic diagram of fabricating SF-G-ART.

Table 1 Response surface factors and levels.

Variation levels	Independent variables (factors)		
	A	B	C
-1	6%	6%	50:1
0	8%	8%	125:1
1	10%	10%	200:1

were treated with liquid nitrogen to obtain a gel having a flat cross section. The dried samples were mounted on sample stubs and sputter-coated with Au, and images were taken using a Scanning Electron Microscope (SEM) (JSM-5610) at 10 kV. The pore size of hydrogel was calculated by Image J according to electron microscopy. FTIR spectroscopic measurements were performed using a Nicolet IS10 system in order to determine any chemical changes that occurred during formulation. Spectra were recorded in the range of 800–4000 cm^{-1} by accumulation of 32 scans. X'Pert PRO MPD X-ray diffractometer (Panalytical, Holland) was used for phase analysis.

2.5. Crosslinking degree test

The crosslinking degree of hydrogel was determined by ninhydrin test (Whitehead et al., 2019). The sample was freeze-dried, added to the configured ninhydrin solution, and placed in a 100 °C water bath for 20 min. At the end of the reaction, 50% isopropanol was added and mixed uniformly. The absorbance of the reaction solution at 570 nm was measured by an UV spectrophotometer (UV-1900, Shimadzu, Japan). The absorbance of glycine solutions with different concentrations were used as the standard. The absorbance of samples without genipin were used as blank control. Calculate the number of free amino acids in each group of hydrogels (A_1) and blanks (A_0) by standard curve. The experiment was conducted in sets

of three ($N = 3$) under identical conditions. The calculation formula of crosslinking degree is shown in (1):

$$\text{Crosslinking degree} = \frac{(A_0 - A_1)}{A_0} \times 100\% \quad (1)$$

2.6. Mechanical property test

The tensile and compressive properties of the hydrogel were tested by Electromechanical Universal Testing Machine. The test was performed at room temperature and standard atmospheric pressure. A lamellar hydrogel (dimensions 5.0 cm \times 1.0 cm \times 0.1 cm) was held between clamps and pulled by top clamp at rate of 5.0 mm/min. A cylindrical hydrogel (diameter 1.0 cm, height 1.0 cm) placed on the bottom disc was pressed down by the top disc at a speed of 10 mm/min and 60% deformation.

2.7. Rheological measurement

The hydrogels were scanned for amplitude and frequency. A parallel plate probe with a diameter of 25 mm was used. Amplitude sweep was performed between 0.1 and 100% strain to obtain the yield point of the gel. Frequency sweep was carried out in the range of 0.01–100 Hz at a constant strain of 1% to obtain storage modulus (G') and loss modulus (G''). All experiments were performed at 25 °C.

2.8. Swelling performance test

The degree of swelling of the hydrogel was evaluated by mass change fraction. The lyophilized hydrogel was weighed (W_0) and placed in a phosphate buffer saline (PBS) of pH = 7.3. The wet hydrogel was allowed to stand and taken out at intervals. The surface moisture was blotted with a filter paper and the hydrogel was weighed (W_1). All experiments were repeated

three times. The calculation formula of degree of swelling is shown in (2):

$$\text{Swelling ratio} = \frac{(W_1 - W_0)}{W_0} \times 100\% \quad (2)$$

2.9. Thermal stability test

The thermal stability of hydrogel was characterized by differential scanning calorimetry (DSC) and thermogravimetric (TG) analysis. DSC test was run at a gas flow rate of 250 mL/min in nitrogen atmosphere. Lyophilized hydrogels powder (3–4 mg) was placed in a sealed aluminum crucible and heated at a rate of 10 °C/min in the range of 30–400 °C. TG test was run at a gas flow rate of 40 mL/min in nitrogen atmosphere. Lyophilized hydrogels powder (6–10 mg) was placed in a sealed aluminum crucible and heated at a rate of 20 °C/min in the range of 40–800 °C.

2.10. Drug Sustained-Release property and pH response performance test

The sample was placed in a test tube with PBS of pH7.4, and incubated at a speed of 120 r/min in a 37 °C incubator. After a certain period of time, the sample was removed and transferred to a new test tube and the new PBS was added for sustained release. Repeat this operation at regular intervals to collect the slow-release solution for each phase. Ultraviolet Spectrophotometry was used to determine the drug content in the sustained-release solution. The specific operation is as follows: The slow-release solution, 95% ethanol, and 0.2% NaOH solution were mixed at a ratio of 1: 2: 5 (v/v/v) and heated for 30 min in a 50 °C shaking water bath. After the reaction solution was extremely cooled, the absorbance was measured at a wavelength of 293 nm. In addition, ART/ethanol solution with equal gradient concentration, PBS and 0.2% sodium hydroxide solution were mixed at a ratio of 2:1:5 (v/v/v), and the absorbance was measured according to the above methods. A standard curve was established with the concentration of each ART solution as the abscissa and the absorbance as the ordinate. The content of ART in the sustained-release solution was calculated according to the standard curve. The slow-release efficiency of ART was calculated according to the following formula:

$$\text{Release rate (\%)} = \frac{(C_1 - C_0)}{C_0} \times 100\% \quad (3)$$

C_0 is the quality of ART in the original sample, C_1 is the quality of ART in the sustained-release solution.

PBS at pH3.4, 4.2 and 6.0 were prepared by phosphoric acid solution. According to the method of testing the sustained-release performance, the drug-releasing performance of the hydrogel in the three different pH solutions was tested under the same conditions.

2.11. In vitro cytocompatibility of SF-G-ART

The experiments were performed by MTS experiments and cell staining experiments to characterize cytocompatibility of hydrogel. The mixed solution before gelatinization was injected into a 96-well plate and incubated to form a hydrogel

sheet with a height of 0.1 cm, and then sterilized by irradiation for 30 min under ultraviolet light. PBS and DMEM were added to the 96-well plate for cleaning. Mouse fibroblasts L929 cells (kept by the State Key Laboratory of Silkworm Genome, Southwest University) (1×10^4 cells/mL) were seeded in each well, and cultured in a 5% CO₂ incubator at 37 °C for 5 days. Cells were cultured in hydrogel-free wells as blank control, and cells in hydrogels without ART were used as negative control. The growth and proliferation of cells were tested by MTS experiments on 1, 3, and 5 days. Cells were stained on the hydrogel at 3 days to observe the cell growth status.

2.12. Anti-inflammatory activity of SF-G-ART

Hydrogels were prepared in a 96-well plate according to 2.11. RAW264.7 cells (1×10^4 cells/mL) were seeded in each well, and 100 μL DMEM or 100 μL DMEM + 0.5 μg/mL LPS were added. Cells cultured in a 5% CO₂ incubator at 37 °C for 1 day. Then Micro NO Content Assay Kit was used to measure the NO release amount of cells in each well. Cells were cultured in hydrogel-free wells as blank control, and cells in hydrogels without ART were used as negative control. The growth and proliferation of cells were tested by MTS experiments.

2.13. In vitro antitumor activity of SF-G-ART

Two cancer cell lines, HepG2 and SMMC7721 (provided by college of pharmaceutical, Southwest University) were used for investigation of *in vitro* antitumor activity. Cancer cells were cultured on the hydrogel, and the growth status of cancer cells was observed by MTS experiment and cell staining experiment to characterize the effect of SF-G-ART on inhibiting tumor growth *in vitro*. The experimental operation is the same as the method of cytocompatibility *in vitro*.

2.14. In vivo evaluation of wound healing

A rat full-thickness skin resection model was established to study the wound healing effect of SF-G-ART. 8-week-old rats (about 250 g) were selected for experiments, and all experiments were performed under sterile conditions. Anesthesia was performed by intraperitoneal injection of a 7% chloral hydrate solution (5 mL/kg). Shaved rats disinfect with alcohol. The wound location was masked with a punch on the back and the entire layer of skin was removed at that location. Three wounds (10 × 10 mm) were made on the back of each rat, and the interval between the wounds was not < 10 mm. The hydrogel (1.5 cm × 1.5 cm × 0.1 cm) was sterilized using UV irradiation. The experimental group (SF-G-ART) was given an external dressing with drug-containing hydrogel, while the control group (SF-G) was given an external dressing with drug-free hydrogel. Hydrogels were changed daily. The blank group done nothing. The wound healing rate (%) is calculated according to the following formula:

$$\text{Wound healing rate (\%)} = \frac{A_0 - A_n}{A_0} \times 100\% \quad (4)$$

A_0 is wound area on day 0, A_n is wound area on day 'n'.

Wound skin was collected in executed rats on days 6, 10, and 18. H&E assay was used for histopathological examination, and immunohistochemical technique was used to determine the expression of related genes.

2.15. *In vivo* evaluation of tumor therapy

A Balb/c nude mouse tumor model of HepG2 cells was established to study the therapeutic effect of hydrogel on tumors. 8-week-old nude mice (about 22 g) were selected for experiments, and all experiments were performed under sterile conditions. HepG2 cells (150 μ L/one mouse) was injected subcutaneously in nude mice to induce tumor growth to 0.1–0.15 cm³. The hydrogel (1.5 cm \times 1.5 cm \times 0.1 cm) was sterilized using UV irradiation. The experimental group (SF-G-ART) was given an external dressing with drug-containing hydrogel, while the control group (SF-G) was given an external dressing with drug-free hydrogel. Hydrogels were changed daily. The blank group had done nothing. Nude mouse body weight were measured twice a week. Tumor formation was observed every three days, and tumor volume was recorded. Blood and tumor tissue were collected in executed nude mice on day 15. H&E assay was used for histopathological examination, and immunohistochemical technique was used to determine the expression of related genes.

2.16. Significance analysis

All statistical analyses were performed by using Origin 9.0 software. Data were presented as mean \pm standard deviation and analyzed by one-way analysis of variance. A *p*-value $<$ 0.05 was denoted as statistically significant. * represents *p* $<$ 0.05, ** represents *p* $<$ 0.01, and *** represents *p* $<$ 0.001.

3. Results and discussions

3.1. Fabrication of SF-G-ART composite hydrogel

In order to fabricate an SF-G-ART composite hydrogel with optimum release effect, 17 experimental formulations were designed based on Box-Behnken Design in RSM. The formula and results obtained by taking three independent factors as independent variables and the ART sustained release effect as response, which are shown in Table S1. A quadratic polynomial fitting was performed through statistical analysis to obtain a prediction model, which represented the effect of each factor and the interaction between the factors on the response when the data was fitted to the equation. The ANOVA results (Table S2) listed for the ART sustained-release rate indicated that the model was significant with *p* value $<$ 0.0001 for calculated responses, while it is not significant with value of *p* = 0.7186. The correspondence figure between the residuals and the prediction of the equation showed a scattered distribution, and the correspondence figure between the predicted value and the actual experimental value showed a linear correlation (Fig. S1), proving that the model fitted well. The influence of each factor and interaction between the dependent variables were shown in two-dimensional contour maps and three-dimensional response surface maps (Fig. S2). The inter-

action between SF concentration and G concentration, G concentration and crosslinking ratio showed significant interactions. Within a limited range of formulas, the optimum content ratio of hydrogel, consisted of 10% SF, 6% G and crosslinking ratio 60:1 (w/w), was determined based on the optimizing results of the independent and dependent variables. Under this condition, the maximum 24 h sustained-release rate was shown. According to this theoretical prediction, the hydrogel was fabricated and its 24 h sustained-release rate of ART in PBS solution was tested. The results showed that the theoretical prediction value of the 24 h sustained-release rate (75.0918%) was similar to tested result, indicating the optimum content ration predicted by RSM was reliable.

3.2. The morphology of hydrogel

To improve the solubility of ART, PEG4000 was introduced to dissolve the ART at first according to our previous study (Dai et al., 2020). On basis of optimum ratio content, the SF solution and the G/ART solution were prepared separately and then mixed together (Fig. 2). After that, the SF-G-ART composite hydrogel was fabricated by crosslinking with genipin, and its optical appearance and microscopic morphology were shown in Fig. 2. SF-G without loading ART was set as a control. SF-G-ART had a uniform appearance without any phase separation. The microscopic morphology exhibited that the lyophilized SF-G-ART (Fig. 2b) and SF-G composite hydrogel (Fig. 2c) exhibited a porous structure while the phase separation of SF-G mixture was observed without crosslinking by genipin. SF-G-ART had an average pore size (diameter) of 83.25 ± 43.65 μ m, while the average pore size of SF-G is around 50.35 ± 19.99 μ m (Fig. 2d and e). Compared to SF-G, the wider distribution and higher diameter of pore size for SF-G-ART probably caused by porogen PEG4000.

Further, the inner structure of the fabricated hydrogel was analyzed by FTIR and the result was shown in Fig. 2g. The characteristic peaks of pure G hydrogel appeared at 1648.8 cm^{-1} , 1542.5 cm^{-1} , and 1242.2 cm^{-1} , which belongs to amide I, amide II, and amide III, respectively. Compared to pure G hydrogel, the absorption peaks of amide I and amide II of SF-G-ART shifted to the lower wavenumber, appeared at 1637.4 cm^{-1} , 1531.2 cm^{-1} , and 1239.3 cm^{-1} , possibly because of the formed amide group between the ester group from genipin and the $-\text{NH}_2$ group from gelatin (Manickam et al., 2014). The characteristic peak of SF-G at 3287.7 cm^{-1} moved to a lower wavenumber and it also became weaker than the corresponding peak (3294.8 cm^{-1}) of SF-G-ART, possibly due to the intense crosslinking between genipin and the primary amine group of SF. Compared with PEG4000, the hydroxyl absorption peak of SF-G-ART at 3437.8 cm^{-1} shifted to 3423.7 cm^{-1} , proving the probable formation of hydrogen bonds based on PEG4000 inside the hydrogel. The characteristic peak of ART was not obvious in the FTIR curve of SF-G-ART, which might resulted from the superposition and influence of the peak of PEG4000. The FTIR analysis demonstrated that the crosslinking network through various chemical and physical interactions was formed inside the SF-G-ART composite hydrogel.

XRD was used to characterize the crystallization of fabricated hydrogel and results were showed in Fig. 2h. The XRD curve of PEG4000 powder showed diffraction peaks at

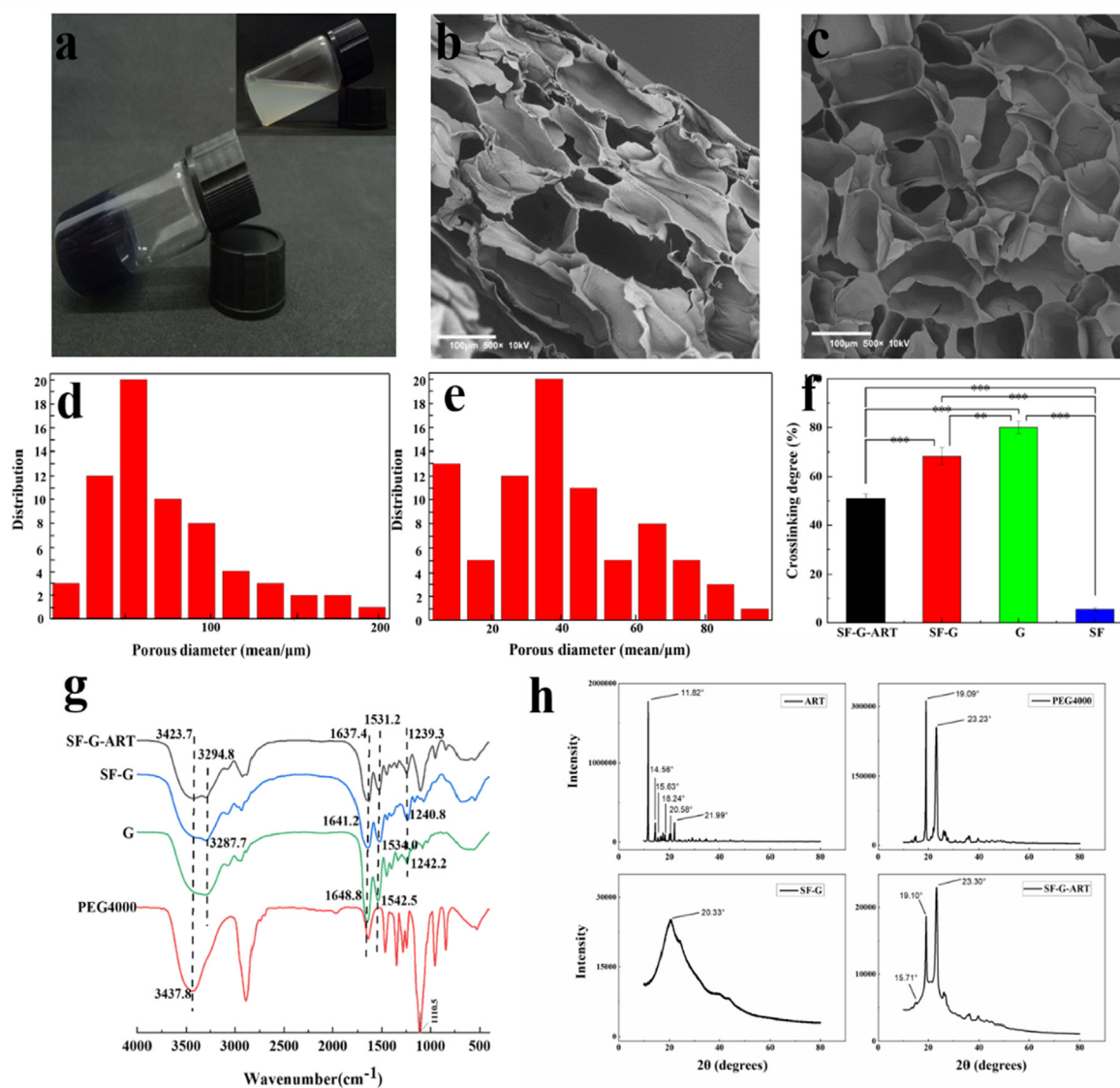


Fig. 2 The morphology and structure of fabricated hydrogels. (a) Optical appearance of SF-G-ART. The image in upper right corner SF-G mixed solution before crosslinking by genipin. (b, c) Cross-section morphology of lyophilized SF-G-ART and SF-G. (d, e) The pore size distribution of SF-G-ART and SF-G. (f) Crosslinking degree of SF-G-ART, SF-G, G hydrogel and SF solution crosslinked by genipin. (g) The FTIR curve of ART, PEG4000, G hydrogel, SF-G and SF-G-ART. (h) The XRD curve of ART powder, PEG4000 powder, SF-G and SF-G-ART lyophilized hydrogel.

19.09°, 23.23° and 26.17°. These diffraction peaks were observed in the SF-G-ART, indicating that PEG4000 partially precipitated as crystals in the hydrogel. The characteristic diffraction peak (11.82°, 14.56°, 15.63°, 18.24°, 20.58° and 21.99°) of ART was not observed in XRD curve of SF-G hydrogel but some of them was observed in XRD curve of SF-G-ART hydrogel (15.71°) though it was little weaker, indicating that ART might form a new crystal structure phase.

3.3. Crosslinking degree of SF-G-ART

Crosslinking degree is highly relating to the properties of hydrogel. Fig. 2f showed the crosslinking degree of fabricated hydrogels. The results showed that through crosslinking reac-

tion by genipin, G hydrogel had the highest crosslinking degree of $80.00 \pm 2.52\%$. With the additional SF, possibly caused by its lower crosslinking efficiency, the crosslinking degree of SF-G significantly decreased to $68.43 \pm 3.29\%$. However, SF also provided the indispensable support through physical reactions like hydrogen bond. The entanglement of the flexible long chain of PEG4000 with other macromolecules may reduce the degree of crosslinking with genipin. As a result, the crosslinking degree was as low as 50.94 ± 1.84 .

3.4. Mechanical property

Wound dressings requires certain mechanical properties especially good elongations when using in joint area so that they

can maintain their integrity and play a role of protection during use [10]. The mechanical properties of the hydrogels were tested to assess the morphological stability (Fig. 3). SF-G was easily broken during the test because it could not withstand the pressure of tensioner chuck. SF-G-ART had better flexibility and ductility and its tensile stress reached 1.42 MPa, and the maximum elongation could reach 124.99%, which can ensure the hydrogel is not easily broken by external forces in use. The compressive stress of SF-G-ART could reach 0.44 MPa, which was significantly greater than that of SF-G (0.09 MPa). SF-G-ART hydrogel had better mechanical properties than that of SF-G and G based hydrogels in published studies no matter for tensile stress and compression resistance, probably resulted from the intertwining effect of PEG4000 (Table 3). PEG4000 is a flexible long-chain molecule and it can be intertwined with G molecules and SF molecules through hydrogen bond, which further supported the three-dimensional network structure and enhanced the mechanical properties of SF-G-ART.

3.5. Rheological measurement

The rheological properties of fabricated hydrogels were characterized by rheometer (Fig. 4a and b). Shear strain (0.1–100%) was used to determine the linear viscoelastic region. In the region of linear viscoelasticity, G' was greater than G'' , that is, the hydrogel had elastic properties, and the elastic response was stronger than the viscous response, which appeared as a solid behavior (Singh et al., 2016b). Compared with the pure G hydrogel, the G' and G'' of SF-G had a little decrease, indicating the less stable network structure. However, the increased G' and G'' of SF-G-ART attribute to the formed inner composite structure by blending SF and PEG4000. And also, SF-G-ART had relatively constant performance over the entire frequency range, exhibiting its frequency stability. These results illustrated that SF-G-ART had a uniform and stable inner structure.

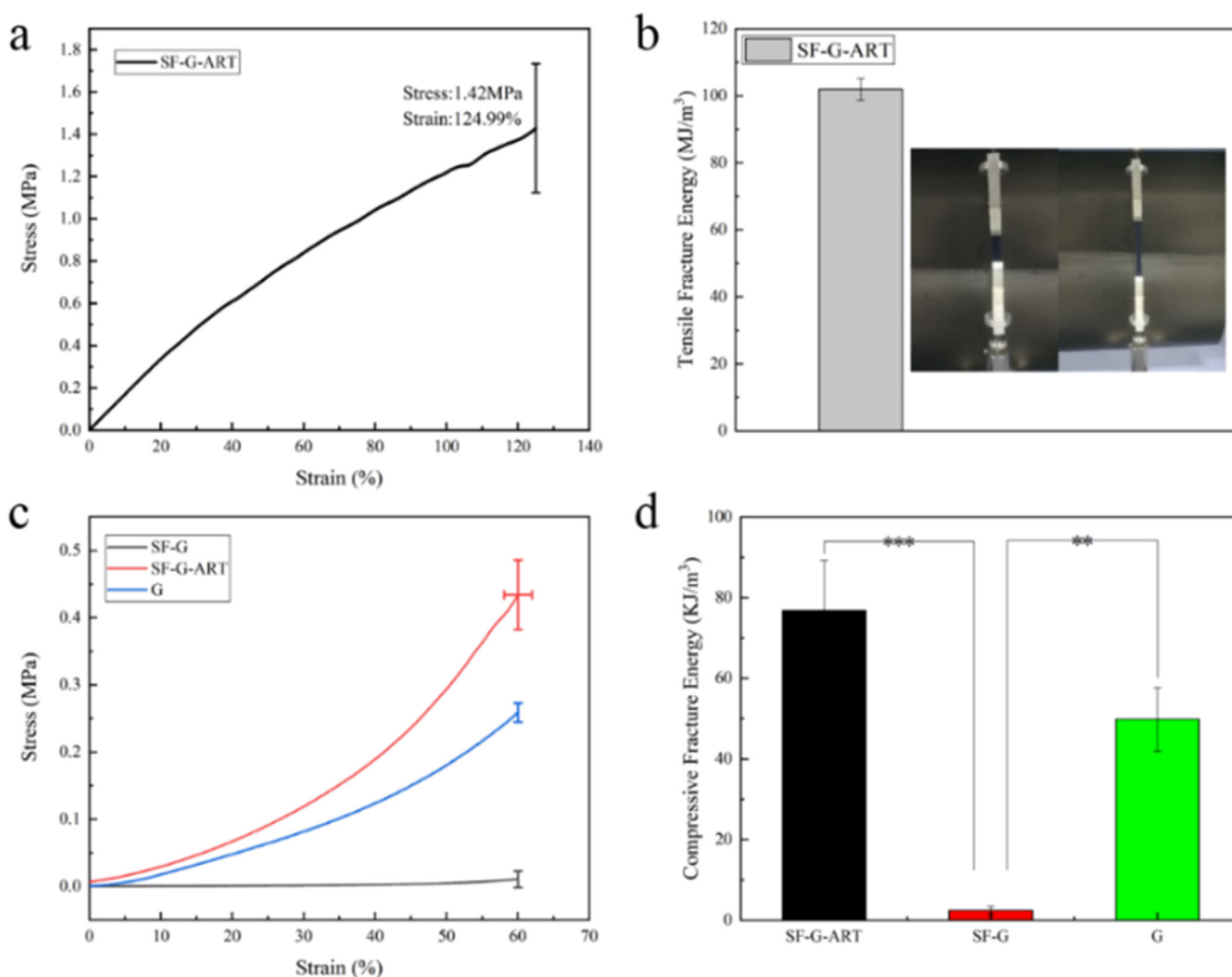


Fig. 3 Mechanical properties of fabricated hydrogels. (a, b) Tensile stress–strain curve and tensile fracture energy of SF-G-ART. (c, d) Stress–strain curve of 60% deformation compression and fracture energy of G hydrogel, SF-G and SF-G-ART. Data are expressed as mean \pm standard deviation of triplicate samples.

Table 3 Mechanical property of gelatin based hydrogels.

Sample	Crosslinking method	Property	Reference
CP/G hydrogel	Physical crosslinking	Improved compression modulus by 9 times compared with pure G Gel	(Lu et al., 2018)
HMG hydrogel	Physical crosslinking	Maximum compressive stress of 5.7 KPa	(Takei et al., 2020)
G hydrogel	Chemical crosslinking by SGDA	Maximum compressive stress of 0.254 MPa	(Kim et al., 2020)
G/HA hydrogel	Chemical crosslinking by EDC/NHS	Tensile stress of 24.91 kPa High flexibility	(Luo et al., 2019)
G hydrogel	Enzymatic crosslinking by mTG	Tensile stress ranging from 18 to 48 kPa	(Dinh et al., 2018)
SF-G-ART hydrogel	Chemical crosslinking by genipin	Tensile stress of 1.42 MPa, compressive stress of 0.44 MPa	This study

3.6. Swelling performance

Hydrogel can absorb extrude from wound and provide a moisture environment for wound healing. Their ability of absorbing and retaining can be reflected by swelling performance. The swelling property test revealing that all fabricated hydrogels

swelled rapidly within the first 2–3 h and reached equilibrium in PBS solution within 5 h (Fig. 4c). Although the pure G hydrogel had high crosslinking degree and swelling ratio (more than 1400%), it could not keep the stable structure for a long time. The swelling ratio of SF-G-ART and SF-G decreased significantly because of the additional SF. The additional SF

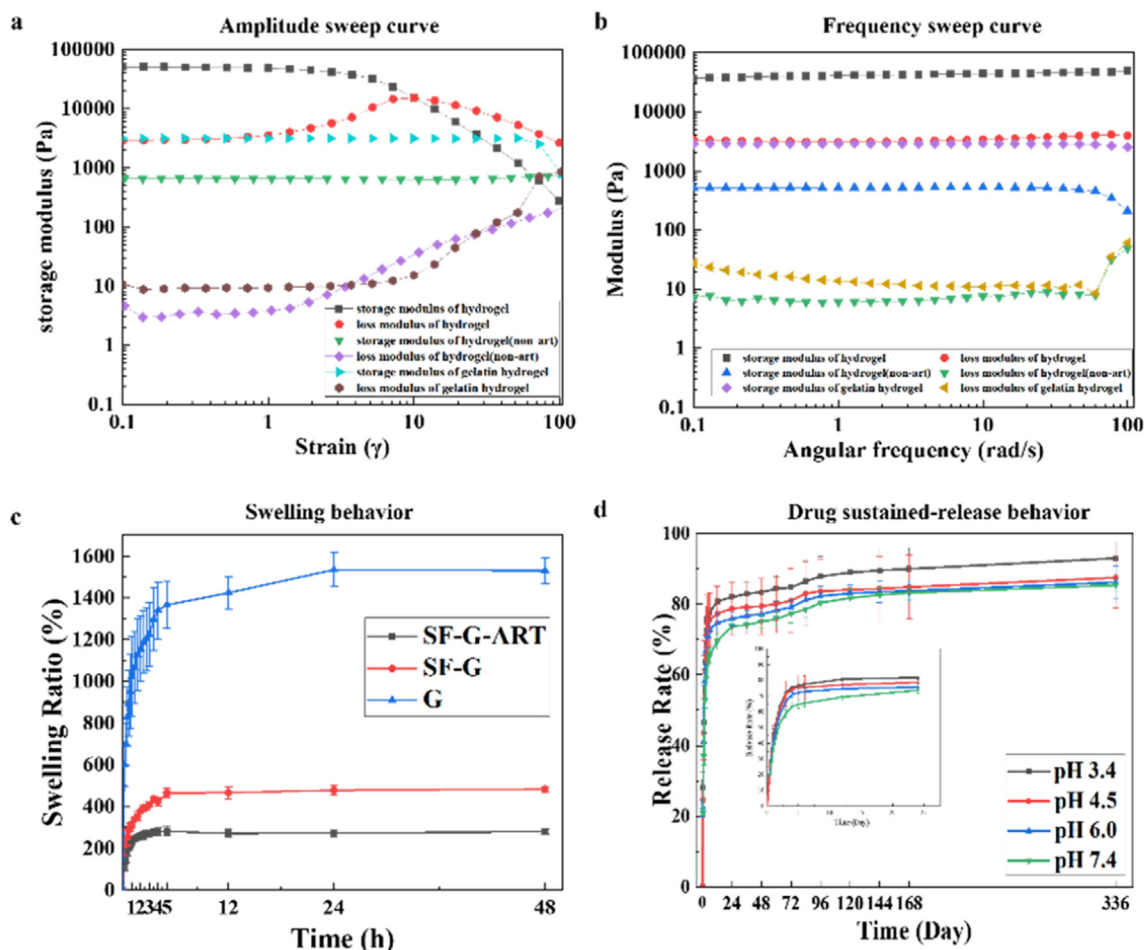


Fig. 4 Characterization of fabricated hydrogels. (a) Amplitude sweep curve of G hydrogel, SF-G and SF-G-ART. (b) Frequency sweep curve of G hydrogel, SF-G and SF-G-ART. (c) Swelling behavior of G hydrogel, SF-G and SF-G-ART. (d) Drug sustained-release behavior in different pH of SF-G-ART. Data are expressed as mean \pm standard deviation of triplicate samples.

formed complex inner structure in composite hydrogel instead of sole structure in G hydrogel, although it caused decreased crosslinking degree of SF-G-ART and SF-G. Further, dissolving of uncrosslinked SF in PBS solution directly made weight of these composite hydrogels reduced and this also affected the structure of composite hydrogel, leading to the decreased swelling ratio. Moreover, the dissolution of PEG4000 also made the swelling ratio declined and the swelling ratio was only round 200%. However, SF-G-ART had a more stable structure and it could maintain the morphology under the equilibrium condition for a long time, which could provide the better support for drug load and release.

3.7. Thermal stability test

Hydrogel prepared by a single component, no matter G or SF, generally has poor stability at high temperature, which probably can be improved in composite hydrogel because of its more complex inner structure. Fig. 5a showed the DSC curve of each fabricated hydrogel, and PEG powder and ART powder was set as control. There were three heat absorption peaks in the DSC curve of SF-G-ART. The sharp endothermic peak at 51.288 °C indicated the melting peak of PEG4000 crystals, and the other two endothermic peaks were the endothermic peaks for the removal of bound water and the decomposition of SF-G-ART, respectively. Possibly because of the inner structure with more crosslinked molecular chains and higher crystal degree, the thermal decomposition temperature of SF-G-ART (281.11 °C) was higher than that of SF-G (276.95 °C) and pure G hydrogel (276.12 °C). No endothermic peak (156.23 °C) of ART powder was found in SF-G-ART, indicating that ART was too tiny to be detected or it was not as a crystal structure in composite hydrogel.

Fig. 5b showed the TGA curve of fabricated hydrogels. All samples had weight loss in two stages. Below 100 °C, the free water molecules absorbed from the air were lost from the hydrogel. The carbon-carbon main chains were broken at about 280–290 °C, and the three-dimensional crosslinked network structure was completely decomposed. The decomposition temperature of SF-G-ART (295.2 °C) was the highest among three fabricated hydrogels, and its residual carbon content was also the heaviest. All the results demonstrated that the SF-G-ART composite hydrogel had the best thermal stability.

3.8. Drug sustained-release property and pH response performance test

The release of ART from SF-G-ART composite was pH sensitive (Fig. 4d). In general, the drug release rate and the accumulative released ART increased as the pH of the solution decreased. At pH3.4, initial burst release occurred within 3 h and the cumulative released ART reached 72.39%. Then, the drug release rate sharply reduced, and the released ART was around 15% within 96 h. The protonation of amino group in composite hydrogel caused electrostatic repulsion in an acidic solution, leading to an enlarged inner network structure of the hydrogel, and this was conducive to the release of ART. After 120 h, SF-G-ART began to decompose. Under the neutral environment (pH7.4), the sustained released ART from SF-G-ART reached as high as 81.744% within 120 h, which can ensure the therapy application of SF-G-ART.

In order to reveal the release mechanism of SF-G-ART, the cumulative release amount of ART (Q) and time (T) in 24 h and 24–120 h were fitted with the release model, including zero-order release model, first-order release model, Higuchi equation and Ritger-Pepper equation (Table S3). The release of ART within 24 h fitted well with the first-order release model (Schwartz et al., 1968). The hydrogel quickly swelled after immersed in the solution, and the ART released diffused and released rapidly inside the three-dimensional structure with the solution absorbed by the hydrogel. Subsequently, the amount of ART released decreased significantly, and the release trend became gentle. The fitting results showed that the release of ART in 24–120 h was in line with the zero-order kinetic equation (Arosio et al., 2008). The release of ART related to the collapse of SF-G-ART. The pH of the solution only affected the amount of ART released, without changing the process and principle.

3.9. In vitro cytocompatibility of SF-G-ART

As a biomedical material, SF-G-ART must have good cytocompatibility. The following results (Fig. 6a and b) were obtained cell experiments. L929 cells were cultured on SF-G-ART and SF-G and the results showed the cells has a good proliferation and viability during 5 days. Although the cell viability of SF-G-ART was slight lower than that of SF-G (day 5), SF-G-ART did not show significant cytotoxicity to the cells. The high concentration of ART, above 0.063 mg/mL, had significantly toxicity to normal cell, according to our previous study (Dai et al., 2020). Further, the observation by confocal microscope showed the cells could attach on the surface of both hydrogels. With the long culture time, the cells could migrate and grow inside both hydrogels, indicating the good cell compatibility of these hydrogels. All of results prove the good biocompatibility of the fabricated SF-G-ART, and this hydrogel can be used as a biomaterial in biomedical field.

3.10. Anti-inflammatory activity of SF-G-ART

Inflammatory process is a requisite stage for wound healing. Relieving inflammatory effect and shortening this process beneficial to wound healing. Thus, hydrogel with anti-inflammatory effect is better to promote wound healing. RAW264.7 cells can release a large amount of NO after induced by LPS. A large amount of NO is toxic to cells or it can react with intracellular substances to generate free radicals, which will hurt biological macromolecules in cells and induce the inflammatory response (Ignarro, 2002; Hussain et al., 2004). According to this principle, RAW264.7 cells were used to test the anti-inflammatory effect of fabricated SF-G-ART. It was found that the amount of NO release was significantly decreased after the cells cultured on SF-G-ART, exhibiting the anti-inflammatory effect of fabricated SF-G-ART (Fig. 6c). Obviously, ART was contribute to the anti-inflammatory effect since SF-G could not reduce the release effect of NO. Its possible mechanism is to interfere with transcriptional signaling pathways of NF- κ B in cells, thereby inhibiting the synthesis of matrix metalloproteinase-3 and NO synthetase, as a result, the generation of NO remarkably cut down (Li et al., 2012). Moreover, the cytocompatibility of the fabricated hydrogels to RAW264.7 cells was tested to

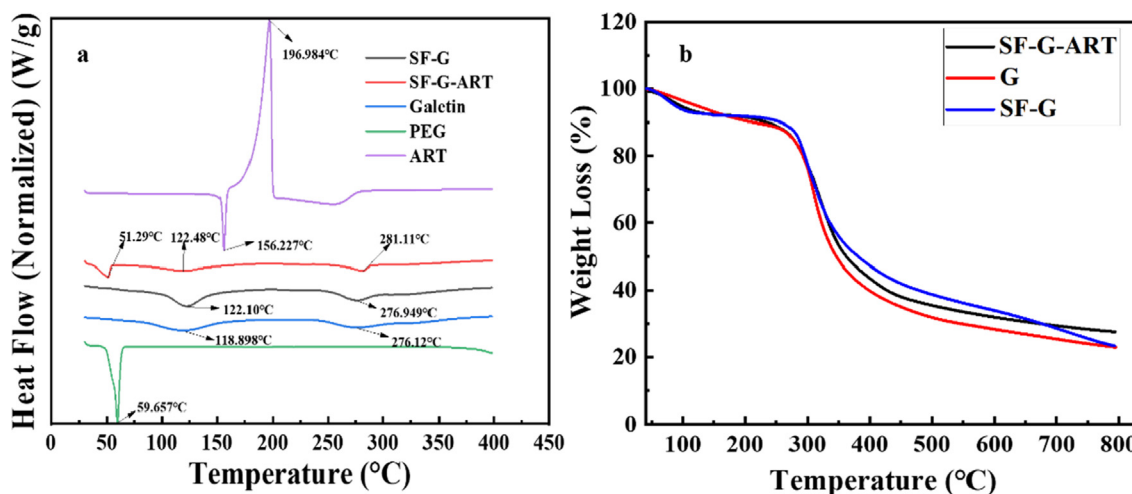


Fig. 5 Thermal stability analysis of fabricated hydrogels. (a) DSC curve. (b) TGA curve.

determine this inhibitory effect come from the inhibitory activity of ART instead of its toxicity to cells (Fig. 6d). The good cell viability indicated SF-G-ART had no cytotoxicity to RAW264.7 cell no matter before or after induction by LPS. These results proved that the release of ART from SF-G-ART could significantly inhibit inflammatory effect without cytotoxicity to RAW264.7 cells.

3.11. *In vitro* antitumor activity of SF-G-ART

Two cancer cell strains, HepG2 and SMMC7721, were selected for determine the antitumor activity of fabricated hydrogels (Fig. 6e–h). Compared with than of SF-G, SF-G-ART exhibited distinct inhibition on HepG2 and SMMC7721 from the first day of culture. The cells viability was as low as 45.3% within 5 days for HepG2 and it was no more than 45.8% for SMMC7721, proving the significant inhibition on both strains of cancer cells *in vitro*. ART has a special peroxy bridge in structure. The cleavage of this peroxy bridge can produce large amount of ROS, which can damage to cancer cells. And this cleavage is highly depend on iron ion. After the peroxy bridge breaks, a large amount of ROS is formed, which results in excessive oxidative damage to DNA of cell (Wang and Yi, 2008). The more iron in cancer cells makes the growth inhibition of cancer cells more significant. This result was consistent with the confocal scan results. The three-dimensional network structure of the hydrogel is conducive to the adhesion growth and localization of cancer cells and increases the inhibition efficiency.

3.12. *In vivo* evaluation of wound healing

The effect of fabricated hydrogels on wound healing was evaluated by animal experiment and the results were shown in Fig. 7.

In the early stage, the wound without treatment had some exudation which likely induce bacterial infection. SF-G and SF-G-ART absorbed the exudate and provided a clean and moist environment for the wound. The scabs on the wounds were formed on the 6th day and they fell off spontaneously on the 10th day. The scabs of the SF-G group and the SF-

G-ART group fell off earlier than blank control group. And for blank group, there still was visible blood exudation around the wound. The fabricated hydrogel promoted the scab to fall off naturally, avoided the infection under the scab, and removed the barriers of epithelialization. On the 18th day, the wound of the SF-G-ART group almost healed and flattened (99.51%) and the wounds of the SF-G group also had a good healing (98.39%), compared with that of the blank control group (96.03%). ART can prevent infection and suppuration through anti-inflammatory effects and the release of ART from SF-G-ART probably shortened the period of inflammatory stage so that accelerated the wound healing.

The wound skin on the 6th day, 10th day and 18th day was analyzed by H&E staining to evaluate wound healing. On the 6th day, infiltration of inflammatory cells was observed in each group. However, the infiltration area in the SF-G-ART group was relatively small, indicating that it had a lower inflammatory response. This proved that the released ART exhibited anti-inflammatory effect, which is beneficial to shortening the inflammation reaction time and accelerating wound healing. On the 10th day, epidermal regeneration happened in each group. Compared with blank control and SF-G group, the SF-G-ART group had more fibroblasts, more regular connective tissue and smoother regenerated epithelium. On the 18th day, the epidermis, cuticle and skin appendages (hair follicles) was formed in all groups. However, the blank group and SF-G group had fewer collagen fibers and thinner epidermis which did not completely cover the wound (red box). The SF-G-ART group formed a more mature epidermis which had better fibrosis and collagenization.

Further, EGF expression was detected to illustrate the role of fabricated composite hydrogels in wound healing (Fig. 7d). On day 6, compared with blank control group, EGF had a stronger and intensive expression in the SF-G-ART and SF-G groups, and it mainly distributed in the outer layer of the wound, which was conducive to the proliferation of fibroblasts and epithelial cells and the formation of epidermis. On the 10th day, the EGF had an intensive expression in each group was positive and it was widely distributed in the dermis layer. The EGF of the blank group mainly concentrated in the basement membrane. And the EGF in SF-G-ART group was

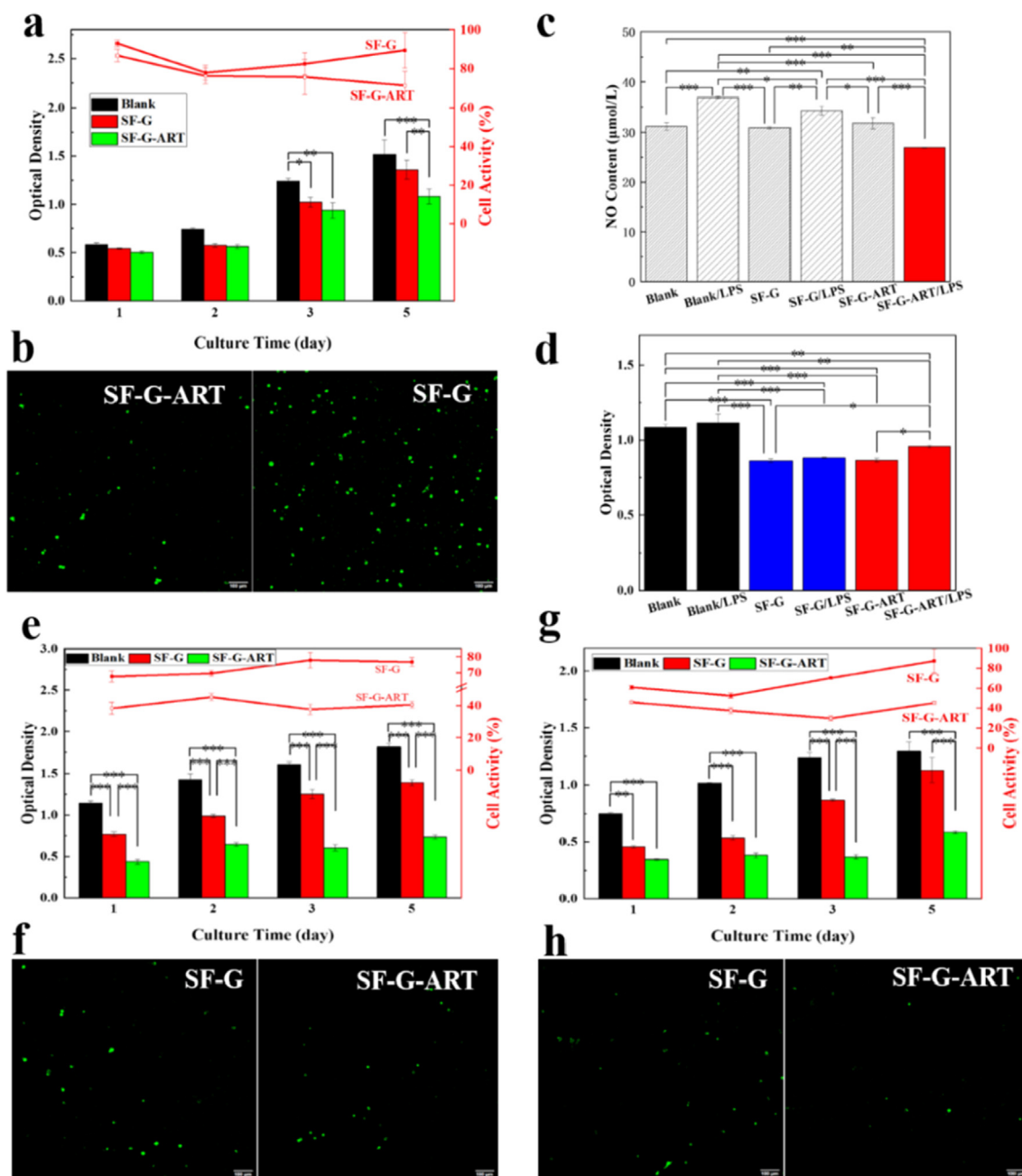


Fig. 6 Biological effect of fabricated hydrogels. (a) Cytotoxicity of ART on normal cell L929 by MTS assay. (b) Life cell staining of L929 cells treated with SF-G and SF-G-ART by confocal microscope. (c) Inhibition of SF-G and SF-G-ART on NO production in LPS-stimulated RAW264.7 cells. (d) Cytotoxicity of SF-G and SF-G-ART on RAW264.7 cells by MTS assay. (e) Effects of SF-G and SF-G-ART on cell viability of HepG2 cancer cells for 5 days. (f) Life cell staining of HepG2 cells treated with SF-G and SF-G-ART by confocal microscope. (g) Effects of SF-G on cell viability of SMMC7721 cancer cells for 5 days. (h) Life cell staining of SMMC7721 cells treated with SF-G and SF-G-ART by confocal microscope. Data are expressed as mean \pm standard deviation of triplicate samples.

evenly expressed in epidermis, basement membrane and collagen fibers. SF-G-ART might stimulate fibroblasts to promote the increase and deposition of collagen fiber by regulating the expression of EGF, thereby promoting the formation of collagen and granulation tissue. On the 18th day, the skin wound was completely closed, and the fibroblasts in the skin tissue were reduced. Therefore, the EGF expression became weaker, resulting in the reduction of collagen fiber synthesis and collagen deposition. Studies have suggested that both EGF and

ART can directly down-regulate the expression of α -smooth muscle actin caused by TGF- β 1 (Park et al., 2000; Wang et al., 2020). Decreased expression of α -smooth muscle actin can reduce the formation of myofibroblasts and the disorderly arrangement of collagen fibers, thereby making the regenerated tissue or skin smoother without hyperplasia or scarring. And in our experiment, ART can regulate the expression of EGF to make it beneficial to wound healing. This may be the reason why the collagen of the SF-G-ART group found

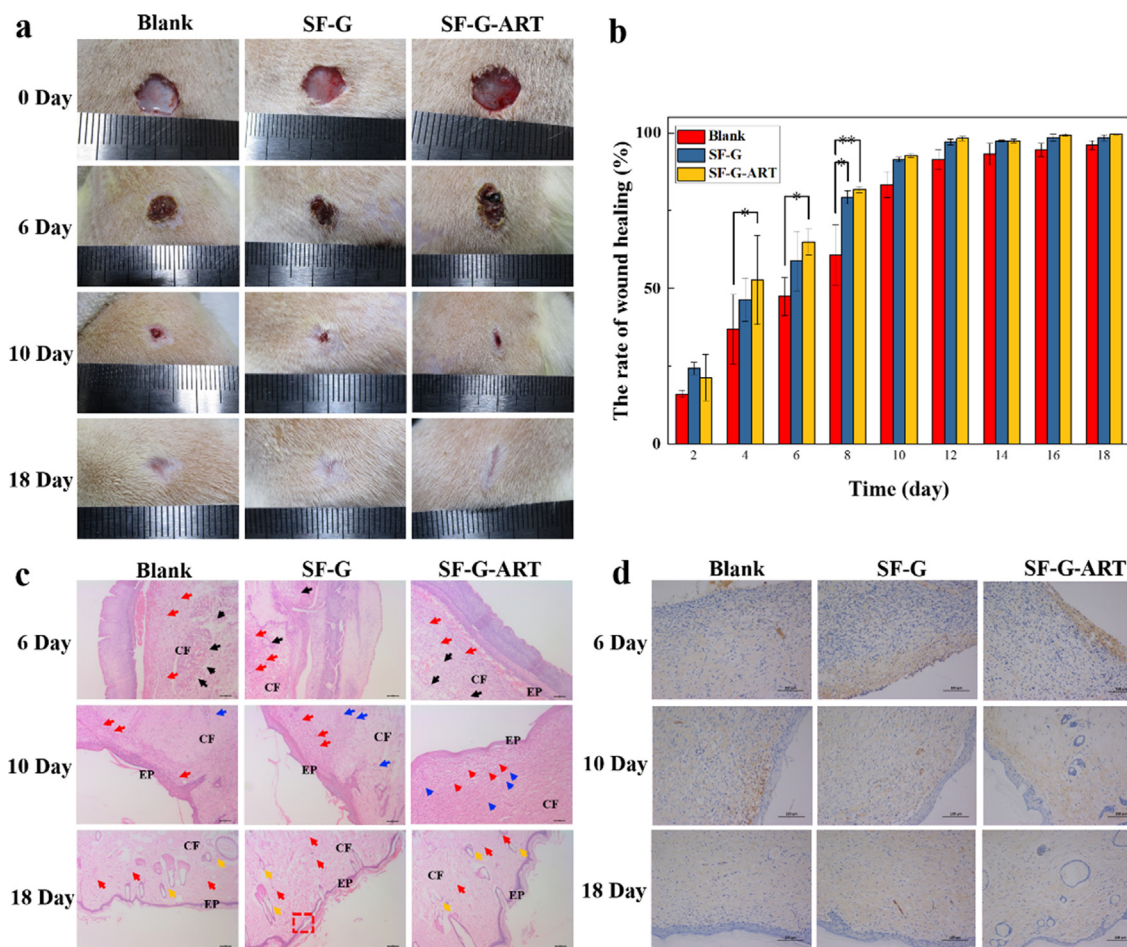


Fig. 7 The effect of fabricated hydrogels on wound healing. (a) Photographs of wounds treated with different hydrogels. (b) Area ratio of wound healing. (c) H&E histological analysis of wounded rats skin on days 6, 10, and 18. Red arrows indicate fibroblasts, black arrows indicate inflammatory cells, blue scissors indicate capillaries, orange arrows indicate hair follicle structure, CF represents collagen fibers and EP represents epidermis. (d) EGF immunohistochemical analysis of rat wounded skin on days 6, 10 and 18. Data are expressed as mean \pm standard deviation of triplicate sample.

in H&E staining was more neatly arranged at each stage. In general, the released ART had an anti-inflammatory effect, which could shorten the inflammation period and further accelerate wound healing so that SF-G-ART exhibited the effect of promoting wound healing.

3.13. *In vivo* evaluation of tumor treatment

Our previous study proved the ART in PEG4000 solution had the apparent antitumor activity (Dai et al., 2020), and SF-G-ART also exhibited the inhibitive effect to HepG2 and SMMC7721 cancer cell *in vitro*. Moreover, a Balb/c nude mouse tumor model of HepG2 cells was established to study the therapeutic effect of fabricated hydrogels on tumors (Fig. 8). SF-G-ART and SF-G were given as an external dressing and the blank group without any treatment was set as a control. On the 15th day, the tumors in SF-G group and blank control group had a rapid growth. The tumors in SF-G-ART group were inhibited and it only grew by 47.62% on the 15th day, which was significantly lower than SF-G group (563.06%) and blank control group (494.42%) (Fig. 8a and b). Apparently, the released ART from SF-G-ART showed a sustainable

inhibitive effect on tumor growth due to its pro-apoptotic effect. Moreover, no significant difference in body weight of nude mice in each group was found within 15 days (Fig. 8c), indicating that SF-G and SF-G-ART had no toxic side effects on the normal growth of nude mice.

The further H&E staining analysis revealed that the tumor morphology of the nude mice in the blank group and the SF-G group was significantly different from that in the SF-G-ART treated group. The tumors in the blank group and SF-G group showed typical tumor pathological features. Tumor cells were tightly arranged and showed heteromorphism, including pathological mitotic division, large nucleus and deep staining. Comparatively, the tumor cells in the SF-G-ART group were sparse and disordered, and their nucleoplasm ratio was improved. Nucleolysis and nucleus shrinkage in this group made the nuclear density significantly lower than that of the other two groups. In addition, there was a clear interstitial separation between cells and damaged extracellular matrix. These results indicated that there were a large number of lysed, atrophied or apoptotic tumor cells and partially necrotic tissues inside the tumor after treated by SF-G-ART. CD31 IHC staining analysis of tumor tissues revealed that the density of

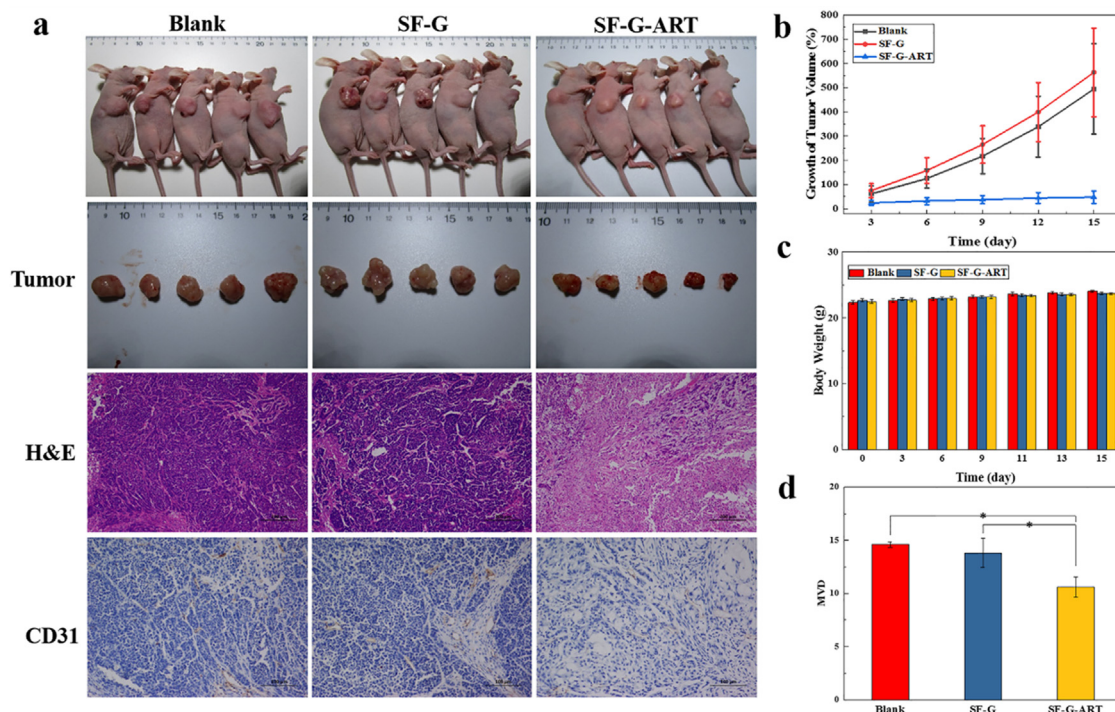


Fig. 8 Tumor therapy of fabricated hydrogels. (a) Tumor photos, H&E staining and CD31 IHC staining after 15 days of treatment with different hydrogels. (b) Growth rate of tumor volume. (c) Changes in body weight of nude mice. (d) Tumor microvessel density after 15 days of treatment with different hydrogels. Data are expressed as mean \pm standard deviation ($n = 5$).

microvessels in tumors of nude mice in SF-G-ART group was significantly lower than that of blank group and SF-G group, indicating that SF-G-ART had the inhibitive effect on angiogenesis in tumor so that it can prevent the exchange of substances for tumor growth and inhibit tumor growth.

In fact, the released ART from SF-G-ART exhibited the inhibitive effect on tumors by possible ways of oxidative toxicity, inhibition of proliferation, induction of apoptosis, and inhibition of new blood vessel formation. The inhibitive way of ART is to induce arrest of G1 cell cycle, reduce the levels of cyclin D1, cyclin E, cyclin dependent kinase 2, cyclin dependent kinase 4 and E2F1, and then up-regulate the expression of CIP1/p21 and Kip1/p27, thus inhibiting the cell cycle process and ultimately inhibiting the proliferation of tumor cells (Hou et al., 2008). ART induces apoptosis of tumor cells by activating caspase-3, increasing Bax/Bcl-2 and poly (ADP-ribose) polymerase, and down-regulating MDM2 oncogene expression (Chen et al., 2018). ART can also regulate gene expression of related angiogenesis factors to inhibit the formation of new blood vessels, such as angiogenin (ANG) and angiogenesis inducer (CYR61) (Anfosso et al., 2006). In general, SF-G-ART exhibited an inhibitory effect on tumors by release of ART, and it has a great potential of application in tumor therapy.

Although the fabricated SF-G-ART exhibits good property of accelerating wound healing and inhibiting tumor growth, its mechanical property and swelling performance should be improved by varying the content of SF and G, or their ratio, even the crosslinking degree in further study. Also, injectable hydrogel based on SF, G and ART must be developed for the better application in cancer therapy *in vivo*.

4. Conclusion

In this study, SF-G-ART composite hydrogel was fabricated through crosslinking effect of genipin. The fabricated SF-G-ART showed good mechanical properties and thermal stability. The loaded ART on this composite hydrogel had favorable sustained-release property, which was a pH sensitive. SF-G-ART composite hydrogel had good biocompatibility. With the biological activity of released ART, SF-G-ART composite hydrogel showed anti-inflammatory property and selective inhibitory effect on tumor cells *in vitro*. Owing to these good properties, SF-G-ART composite hydrogel could accelerate wound healing and significantly inhibit tumor growth *in vivo* experiments. These results prove that SF-G-ART composite hydrogel has a good potential for application in wound dressing and tumor therapy.

CRedit authorship contribution statement

Yu Bao: Conceptualization, Methodology, Investigation, Data curation, Writing – original draft. **Hai-qiang Zhang:** Software, Investigation, Validation. **Li Chen:** Investigation, Formal analysis. **Hai-Hua Cai:** Methodology, Investigation. **Zu-Lan Liu:** Investigation. **Yan Peng:** Resources. **Zhi Li:** Conceptualization, Writing – original draft, Writing – review & editing. **Fang-Yin Dai:** Supervision, Writing – review & editing.

Declaration of Competing Interest

The authors declare that they have no known competing financial interests or personal relationships that could have appeared to influence the work reported in this paper.

Acknowledgements

This research was funded by grants from the National Natural Science Foundation of China (No. 31830094), Funds of China Agriculture Research System (No. CARS-18-ZJ0102) and the Innovation Program for Chongqing's Overseas Returnees (No. cx2019090).

Appendix A. Supplementary material

Supplementary material to this article can be found online at <https://doi.org/10.1016/j.arabjc.2023.104782>.

References

- Ahmadian, E., Eftekhari, A., Dizaj, S.M., Sharifi, S., Mokhtarpour, M., Nasibova, A.N., Khalilov, R., Samiei, M., 2019. The effect of hyaluronic acid hydrogels on dental pulp stem cells behavior. *Int. J. Biol. Macromol.* 140, 245–254. <https://doi.org/10.1016/j.ijbiomac.2019.08.119>.
- Anfosso, L., Efferth, T., Albini, A., Pfeffer, U., 2006. Microarray expression profiles of angiogenesis-related genes predict tumor cell response to artemisinins. *Pharmacogenomics J.* 6, 269–278. <https://doi.org/10.1038/sj.tpj.6500371>.
- Arosio, P., Busini, V., Perale, G., Moscatelli, D., Masi, M., 2008. A new model of resorbable device degradation and drug release - part I: zero order model. *Polym. Int.* 57, 912–920. <https://doi.org/10.1002/pi.2425>.
- Barradell, L.B., Fitton, A., 1995. Artesunate: a review of its pharmacology and therapeutic efficacy in the treatment of malaria. *Drugs* 50, 714–741. <https://doi.org/10.2165/00003495-199550040-00009>.
- Broderick, E.P., O'Halloran, D.M., Rochev, Y.A., Griffin, M., Collighan, R.J., Pandit, A.S., 2005. Enzymatic stabilization of gelatin-based scaffolds. *J. Biomed. Mater. Res. Part B*, 37–42. <https://doi.org/10.1002/jbm.b.30119>.
- Capanema, N.S.V., Mansur, A.A.P., de Jesus, A.C., Carvalho, S.M., de Oliveira, L.C., Mansur, H.S., 2018. Superabsorbent crosslinked carboxymethyl cellulose-PEG hydrogels for potential wound dressing applications. *Int. J. Biol. Macromol.* 106, 1218–1234. <https://doi.org/10.1016/j.ijbiomac.2017.08.124>.
- Chen, J., Zhang, L., Hao, M., 2018. Effect of artemisinin on proliferation and apoptosis-related protein expression in vivo and in vitro. *Saudi J. Biol. Sci.* 25, 1488–1493. <https://doi.org/10.1016/j.sjbs.2018.04.003>.
- Dai, F., Bao, Y., Li, Z., Chen, S.H., Gao, L.Z., Liu, Z.L., Cheng, L., Peng, Y., Tong, X.L., 2020. Artemisinin is highly soluble in polyethylene Glycol 4000 and such solution has multiple biological effects. *Acta Biochim. Pol.* 67, 203–211. https://doi.org/10.18388/abp.2020_5190.
- Dinh, T.N., Hou, S.J., Park, S., Shalek, B.A., Jeong, K.J., 2018. Gelatin Hydrogel Combined with Polydopamine Coating To Enhance Tissue Integration of Medical Implants. *ACS Biomater. Sci. Eng.* 4, 3471–3477. <https://doi.org/10.1021/acsbomaterials.8b00886>.
- Dong, Z.Y., Wu, D., Engqvist, H., Luo, J., Persson, C., 2021. Silk fibroin hydrogels induced and reinforced by acidic calcium phosphate-A simple way of producing bioactive and drug-loadable composites for biomedical applications. *Int. J. Biol. Macromol.* 193, 433–440. <https://doi.org/10.1016/j.ijbiomac.2021.10.160>.
- Eftekhari, A., Dizaj, S.M., Sharifi, S., Salatin, S., Saadat, Y.R., Vahed, S.Z., Samiei, M., Ardalan, M., Rameshrad, M., Ahmadian, E., Cucchiari, M., 2020. The Use of Nanomaterials in Tissue Engineering for Cartilage Regeneration; Current Approaches and Future Perspectives. *Int. J. Mol. Sci.* 21, 536. <https://doi.org/10.3390/ijms21020536>.
- Fan, Z.J., Liu, B., Wang, J.Q., Zhang, S.Y., Lin, Q.Q., Gong, P.W., Ma, L.M., Yang, S.R., 2014. A Novel Wound Dressing Based on Ag/Graphene Polymer Hydrogel: Effectively Kill Bacteria and Accelerate Wound Healing. *Adv. Funct. Mater.* 24, 3933–3943. <https://doi.org/10.1002/adfm.201304202>.
- Florczak, A., Deptuch, T., Kucharczyk, K., Dams-Kozłowska, H., 2021. Systemic and Local Silk-Based Drug Delivery Systems for Cancer Therapy. *Cancers* 13, 5389. <https://doi.org/10.3390/cancers13215389>.
- Guo, Y.Q., An, X.L., Fan, Z.J., 2021. Aramid nanofibers reinforced polyvinyl alcohol/tannic acid hydrogel with improved mechanical and antibacterial properties for potential application as wound dressing. *J. Mech. Behav. Biomed.* 118, 104452. <https://doi.org/10.1016/j.jmbbm.2021.104452>.
- Hou, J., Wang, D., Zhang, R., Wang, H., 2008. Experimental therapy of hepatoma with artemisinin and its derivatives: In vitro and in vivo activity, chemosensitization, and mechanisms of action. *Clin. Cancer Res.* 14, 5519–5530. <https://doi.org/10.1158/1078-0432.Ccr-08-0197>.
- Huang, H.F., He, D.Q., Liao, X.Z., Zeng, H.J., Fan, Z.J., 2021. An excellent antibacterial and high self-adhesive hydrogel can promote wound fully healing driven by its shrinkage under NIR. *Mater. Sci. Eng. C-Mater.* 129, 112395. <https://doi.org/10.1016/j.msec.2021.112395>.
- Hussain, S.P., Trivers, G.E., Hofseth, L.J., He, P.J., Shaikh, I., Mechanic, L.E., Doja, S., Jiang, W.D., Subleski, J., Shorts, L., Haines, D., Laubach, V.E., Wiltrout, R.H., Djurickovic, D., Harris, C.C., 2004. Nitric oxide, a mediator of inflammation, suppresses tumorigenesis. *Cancer Res.* 64, 6849–6853. <https://doi.org/10.1158/0008-5472.can-04-2201>.
- Ignarro, L.J., 2002. Nitric oxide as a unique signaling molecule in the vascular system: A historical overview. *J. Physiol. Pharmacol.* 53, 503–514. <https://doi.org/10.1152/jn.00299.2002>.
- Kapoor, S., Kundu, S.C., 2016. Silk protein-based hydrogels: Promising advanced materials for biomedical applications. *Acta Biomater.* 31, 17–32. <https://doi.org/10.1016/j.actbio.2015.11.034>.
- Kim, S., Jeong, D., Lee, H., Kim, D., Jung, S., 2020. Succinoglycan dialdehyde-reinforced gelatin hydrogels with toughness and thermal stability. *Int. J. Biol. Macromol.* 149, 281–289. <https://doi.org/10.1016/j.ijbiomac.2020.01.228>.
- Koo, H.J., Lim, K.H., Jung, H.J., Park, E.H., 2006. Anti-inflammatory evaluation of gardenia extract, geniposide and genipin. *J. Ethnopharmacol.* 103, 496–500. <https://doi.org/10.1016/j.jep.2005.08.011>.
- Kumar, A., Behl, T., Chadha, S., 2020a. A rationalized and innovative perspective of nanotechnology and nanobiotechnology in chronic wound management. *J. Drug Deliv. Sci. Tech.* 60, 101930. <https://doi.org/10.1016/j.jddst.2020.101930>.
- Kumar, A., Jaiswal, M., 2016. Design and in vitro investigation of nanocomposite hydrogel based in situ spray dressing for chronic wounds and synthesis of silver nanoparticles using green chemistry. *J. Appl. Polym. Sci.* 133, 43260. <https://doi.org/10.1002/app.43260>.
- Kumar, A., Behl, T., Chadha, S., 2020b. Synthesis of physically crosslinked PVA/Chitosan loaded silver nanoparticles hydrogels with tunable mechanical properties and antibacterial effects. *Int. J. Biol. Macromol.* 149, 1262–1274. <https://doi.org/10.1016/j.ijbiomac.2020.02.048>.
- Li, T., Chen, H., Wei, N., Mei, X., Zhang, S., Liu, D.-L., Gao, Y., Bai, S.-F., Liu, X.-G., Zhou, Y.-X., 2012. Anti-inflammatory and immunomodulatory mechanisms of artemisinin on contact hypersensitivity. *Int. Immunopharmacol.* 12, 144–150. <https://doi.org/10.1016/j.intimp.2011.11.004>.
- Li, X., Gu, S., Sun, D., Dai, H., Chen, H., Zhang, Z., 2018. The selectivity of artemisinin-based drugs on human lung normal and cancer cells. *Environ. Toxicol. Pharmacol.* 57, 86–94. <https://doi.org/10.1016/j.etap.2017.12.004>.
- Lu, Q.L., Zhang, S.H., Xiong, M.C., Lin, F.C., Tang, L.R., Huang, B., Chen, Y.D., 2018. One-pot construction of cellulose-gelatin

- supramolecular hydrogels with high strength and pH-responsive properties. *Carbohydr. Polym.* 196, 225–232. <https://doi.org/10.1016/j.carbpol.2018.05.020>.
- Luo, J.W., Liu, C., Wu, J.H., Lin, L.X., Fan, H.M., Zhao, D.H., Zhuang, Y.Q., Sun, Y.L., 2019. In situ injectable hyaluronic acid/gelatin hydrogel for hemorrhage control. *Mater. Sci. Eng. C-Mater.* 98, 628–634. <https://doi.org/10.1016/j.msec.2019.01.034>.
- Luo, J., Zhu, W., Tang, Y., Cao, H., Zhou, Y., Ji, R., Zhou, X., Lu, Z., Yang, H., Zhang, S., Cao, J., 2014. Artemisinin derivative artesunate induces radiosensitivity in cervical cancer cells in vitro and in vivo. *Radiat. Oncol.* 9, 84. <https://doi.org/10.1186/1748-717x-9-84>.
- Manickam, B., Sreedharan, R., Elumalai, M., 2014. 'Genipin' - The Natural Water Soluble Cross-linking Agent and Its Importance in the Modified Drug Delivery Systems: An Overview. *Curr. Drug Deliv.* 11, 139–145. <https://doi.org/10.2174/15672018113106660059>.
- Moeini, A., Pedram, P., Makvandi, P., Malinconico, M., d'Ayala, G. G., 2020. Wound healing and antimicrobial effect of active secondary metabolites in chitosan-based wound dressings: A review. *Carbohydr. Polym.* 233. [https://doi.org/10.1016/j-carbpol.2020.115839](https://doi.org/10.1016/j.carbpol.2020.115839) 115839.
- Natesan, S., Ponnusamy, C., Sugumaran, A., Chelladurai, S., Palaniappan, S.S., Palanichamy, R., 2017. Artemisinin loaded chitosan magnetic nanoparticles for the efficient targeting to the breast cancer. *Int. J. Biol. Macromol.* 104, 1853–1859. <https://doi.org/10.1016/j.ijbiomac.2017.03.137>.
- Park, J.S., Kim, J.Y., Cho, J.Y., Kang, J.S., Yu, Y.H., 2000. Epidermal growth factor (EGF) antagonizes transforming growth factor (TGF)-beta 1-induced collagen lattice contraction by human skin fibroblasts. *Biol. Pharm. Bull.* 23, 1517–1520.
- Schwartz, J.B., Simonelli, A.P., Higuchi, W.I., 1968. Drug release from wax matrices. I. Analysis of data with first-order kinetics and with diffusion-controlled model. *J. Pharm. Sci.* 57, 274. <https://doi.org/10.1002/jps.2600570206>.
- Sharma, P., Kumar, A., Dey, A.D., Behl, T., Chadha, S., 2021. Stem cells and growth factors-based delivery approaches for chronic wound repair and regeneration: A promise to heal from within. *Life Sci.* 268, 118932. <https://doi.org/10.1016/j.lfs.2020.118932>.
- Singh, Y.P., Bhardwaj, N., Mandal, B.B., 2016b. Potential of Agarose/Silk Fibroin Blended Hydrogel for in Vitro Cartilage Tissue Engineering. *ACS Appl. Mater. Interfaces* 8, 21236–21249. <https://doi.org/10.1021/acsami.6b08285>.
- Singh, B., Varshney, L., Francis, S., Rajneesh., 2016a. Designing tragacanth gum based sterile hydrogel by radiation method for use in drug delivery and wound dressing applications. *Int. J. Biol. Macromol.* 88, 586–602. <https://doi.org/10.1016/j.ijbiomac.2016.03.051>.
- Sung, H.W., Liang, I.L., Chen, C.N., Huang, R.N., Liang, H.F., 2001. Stability of a biological tissue fixed with a naturally occurring crosslinking agent (genipin). *J. Biomed. Mater. Res.* 55, 538–546. [https://doi.org/10.1002/1097-4636\(20010615\)55:4<538::Aid-jbm1047>3.3.Co;2-u](https://doi.org/10.1002/1097-4636(20010615)55:4<538::Aid-jbm1047>3.3.Co;2-u).
- Takei, T., Yoshihara, R., Danjo, S., Fukuhara, Y., Evans, C., Tomimatsu, R., Ohzuno, Y., Yoshida, M., 2020. Hydrophobically-modified gelatin hydrogel as a carrier for charged hydrophilic drugs and hydrophobic drugs. *Int. J. Biol. Macromol.* 149, 140–147. <https://doi.org/10.1016/j.ijbiomac.2020.01.227>.
- Wang, Y., Wang, Y., You, F., Xue, J., 2020. Novel use for old drugs: The emerging role of artemisinin and its derivatives in fibrosis. *Pharmacol. Res.*, 104829 <https://doi.org/10.1016/j.phrs.2020.104829>.
- Wang, J., Yi, J., 2008. Cancer cell killing via ROS To increase or decrease, that is the question. *Cancer Biol. Ther.* 7, 1875–1884. <https://doi.org/10.4161/cbt.7.12.7067>.
- Whitehead, F.A., Paramita, V.D., Teimouri, S., Young, S., Kasapis, S., 2019. Controlled release of ascorbic acid from genipin-crosslinked gelatin matrices under moving boundary conditions. *Food Hydrocoll.* 89, 171–179. <https://doi.org/10.1016/j.foodhyd.2018.10.026>.
- Wu, Y., Tang, W., Zuo, J., 2016. Development of artemisinin drugs in the treatment of autoimmune diseases. *Sci. Bull.* 61, 37–41. <https://doi.org/10.1007/s11434-015-0975-9>.
- Xie, Y., Liao, X., Zhang, J., Yang, F., Fan, Z., 2018. Novel chitosan hydrogels reinforced by silver nanoparticles with ultrahigh mechanical and high antibacterial properties for accelerating wound healing. *Int. J. Biol. Macromol.* 119, 402–412. <https://doi.org/10.1016/j.ijbiomac.2018.07.060>.
- Yoon, D.S., Lee, Y., Ryu, H.A., Jang, Y., Lee, K.-M., Choi, Y., Choi, W.J., Lee, M., Park, K.M., Park, K.D., Lee, J.W., 2016. Cell recruiting chemokine-loaded sprayable gelatin hydrogel dressings for diabetic wound healing. *Acta Biomater.* 38, 59–68. <https://doi.org/10.1016/j.actbio.2016.04.030>.
- Zhang, X.H., Yin, Z.R., Guo, Y.Q., Huang, H.F., Zhou, J.Y., Wang, L., Bai, J.Y., Fan, Z.J., 2020. A facile and large-scale synthesis of a PVA/chitosan/collagen hydrogel for wound healing. *New J. Chem.* 44, 20776–20784. <https://doi.org/10.1039/d0nj04016a>.